



# Experimental Research on the Carbon Dioxides Reduction Potential by Substitution Gasoline with Ethanol and Propane Under Reactivity Controlled Compression Ignition in a Single Cylinder Engine

Jeongwoo Lee<sup>1</sup> · Sanghyun Chu<sup>2</sup> · Jaegu Kang<sup>2</sup> · Kyoungdoug Min<sup>2</sup>

Received: 7 September 2023 / Revised: 10 October 2023 / Accepted: 23 October 2023 / Published online: 3 March 2024  
© The Author(s) 2024

## Abstract

In this experiment, it was experimentally investigated the combustion and exhaust characteristics, as well as the thermal efficiency, of RCCI combustion using gasoline, ethanol, and propane as low-reactivity fuels under four operating conditions. For each operating condition,  $gISNO_x$  was limited to 0.15 g/kWh, and  $gISSmoke$  was limited to below 15 mg/kWh. The experiment was conducted by determining the operating conditions that satisfied these limitations and resulted in the highest city thermal efficiency. The low-reactivity fuels were supplied by port injection, while diesel was directly injected into the combustion chamber using a diesel injector. As a result, when gasoline is replaced with low-carbon fuels like ethanol and propane, the reduction in  $CO_2$  emissions occurred. Under maximum power conditions, using ethanol allowed for a maximum reduction in  $CO_2$  emissions of 6.81%. Depending on the driving conditions, ethanol showed a reduction ranging from 3.60 to 6.81%, while propane exhibited a reduction ranging from 3.10 to 5.64%. Additionally, by substituting with ethanol and propane, the GIE could be improved up to 44.73 and 43.56%, respectively.

**Keywords** Carbon dioxides ( $CO_2$ ) · Dual-fuel combustion · Ethanol · Gasoline · Propane · Reactivity controlled compression ignition (RCCI)

## List of Symbols

AFR	Air to fuel ratio
°ATDC	After top dead center
°BTDC	Before top dead center
CI	Compression ignition
CN	Cetane number
CNG	Compressed natural gas
CO	Carbon monoxide
$CO_2$	Carbon dioxides
CR	Compression ratio
EGR	Exhaust gas recirculation
FC	Fuel-cell
GIE	Gross indicated thermal efficiency
$gIMEP$	Gross indicated mean effective pressure

$gISxx$	Gross indicated specific xx emissions
HR	Heat release
HRR	Heat release rate
ICE	Internal combustion engine
ID	Ignition delay
LHV	Low heating value
$MFB_x$	Mass fraction burned $x\%$
$NO_x$	Nitrogen oxides
PCI	Premixed compression ignition
PFI	Port fuel injection
$P_{in}$	Intake pressure
$P_{max}$	The maximum in-cylinder pressure
$PRR_{max}$	(The) Maximum in-cylinder pressure rise rate
RCCI	Reactivity controlled compression ignition
RON	Research Octane number
SI	Spark ignition
SOC	Start of combustion
SOI	Start of (diesel) injection
THC	Total hydrocarbon
$\Phi$	Equivalence ratio

✉ Kyoungdoug Min  
kadmin@snu.ac.kr

<sup>1</sup> Department of Autonomous Vehicle System Engineering, Chungnam National University, Daejeon 34134, Republic of Korea

<sup>2</sup> Department of Mechanical Engineering, Seoul National University, Seoul 08826, Republic of Korea

## Introduction

According to the Special Report on “Global Warming of 1.5 °C” released by the Intergovernmental Panel on Climate Change (IPCC) in 2018, countries around the world are making efforts towards carbon neutrality (IPCC special report, 2018). Particularly in the transportation sector, which accounts for approximately 16% of global carbon dioxide emissions, there is a push to move away from fossil fuel-based power sources (Climate Watch, 2020). In principle, there are three main approaches to reducing carbon dioxide emissions in the power sector.

The first approach is to utilize zero-carbon fuels. Recently, there has been growing interest in fuels such as hydrogen and ammonia, which do not contain carbon in their composition and, therefore, do not produce carbon emissions. The use of fuel-cells (FCs) with hydrogen as the main fuel source, as well as the development of ammonia combustion engines and gas turbines in the maritime and power generation sectors, are being explored. However, hydrogen is difficult to liquefy and has storage challenges, while ammonia has a lower heat value per unit mass (approximately 18.6 MJ/kg) compared to conventional fossil fuels and safety issues related to toxicity. Additionally, ammonia combustion presents challenges such as slow flame propagation speed (approximately 0.07 m/s @ stoichiometric condition) and relatively high minimum ignition energy (approximately 8 mJ @ stoichiometric condition) that need to be addressed (Ayman et al., 2022).

The second approach involves using fuels that contain carbon but capturing the carbon emitted into the atmosphere, effectively reducing the overall carbon emissions to zero using net-zero methods. There is increasing interest in the production of ‘synthetic fuels, known as ‘Electricity based fuel’ (E-fuel), using captured carbon or carbon dioxide and renewable energy (Lee & Lee, 2022). One advantage of E-fuels is that they can be immediately utilized in existing internal combustion engines (ICEs) without major modifications. However, the use of E-fuels requires the precondition that all the energy required for carbon capture, hydrogen production, and their synthesis must come from renewable sources. Furthermore, if conventional carbon-emitting energy sources like thermal power generation are used in any stage of the process, the meaning of net-zero is compromised. Another drawback is that methanol, which is relatively easy to produce through E-fuel synthesis, has a disadvantage of having less than half the heat value compared to conventional fossil fuels when used as a primary oxidized fuel.

Therefore, the third approach, which focuses on improving energy conversion efficiency, needs to be implemented

to maximize the effectiveness of the second approach. Increasing energy conversion efficiency is fundamentally crucial as it allows for longer driving distances with the same level of carbon dioxide emissions.

If it is difficult to replace all existing power sources with zero-carbon fuels in the current situation, research on the utilization of low-carbon fuels such as methanol, ethanol, methane, and propane based on E-fuels is needed. These low-carbon fuels, especially methanol and ethanol, have low auto-ignition characteristics and good vaporization properties, making them suitable for use in spark-ignition engines if used individually. However, spark-ignition (SI) combustion engines are often operated at relatively low compression ratios due to concerns about abnormal combustion such as knocking or pre-ignition (Heywood, 1988). Therefore, it is inevitable that the thermodynamically expected thermal efficiency will be low. To apply these fuels at relatively high compression ratios, it would be beneficial to use them in a dual-fuel combustion system together with high-reactivity fuels like diesel.

In order to implement dual-fuel combustion in compression-ignition (CI) engines, the typical approach is to reduce the fraction of diesel fuel and replace it with low-reactivity fuels in proportion to the reduced energy content, so that diesel acts as the ignition source while the main energy generation is done by the low-reactivity fuel (Karim, 1980, 2015; Reitz & Duraisamy, 2015). In particular, rather than pre-mixing the fuels before supplying them to the engine, a dual-fuel combustion system utilizes separate fuel injection systems for the two different fuels to control the ratio between them inside the combustion chamber. This approach is commonly adopted by dual-fuel engines used in maritime applications.

In the twentieth century, the main approach to dual-fuel combustion in conventional diesel engines involved supplying low-reactivity fuel, such as through port injection, alongside regular diesel combustion. In other words, it was a simple concept of reducing the diesel fraction and compensating with low-reactivity fuel proportional to the reduced energy. According to research by Karim et al., dual-fuel combustion consists of three stages (Karim, 1980). First, the diffusion flame of the highly reactive diesel fuel occurs. Second, the low-reactivity fuel contained in the diesel spray is combusted. Finally, the combustion propagates through the distributed low-reactivity fuel in the surrounding area. This fuel substitution method has achieved significant reduction in smoke emissions, but it has also led to increased nitrogen oxide (NO<sub>x</sub>) emissions compared to conventional gasoline spark ignition (SI) combustion due to increased premixed ratio. Additionally, the combustion involving low-reactivity fuels that are unable to participate in the combustion process, such as due to crevices, has posed problems in terms of total hydrocarbon emissions (Felayati et al., 2021; Lee

et al., 2015). Moreover, the premixed low-reactivity fuels have caused knocking issues under high load conditions.

Therefore, in the twenty-first century, a dual-fuel PCI (Premixed Compression Ignition) approach was introduced by Inagaki et al., which not only incorporates low-reactivity fuels but also blends them with diesel fuel to achieve combustion based on premixed mixtures (Inagaki et al., 2006). The diesel injection timing is advanced to the mid-to-late compression phase, earlier than the top dead center, to achieve a stratification of reactivity between diesel and low-reactivity fuel (in the mentioned paper, iso-octane) and enable smoother HCCI (Homogeneous Charge Compression Ignition) combustion.

A derived approach is the RCCI (Reactivity Controlled Compression Ignition) method proposed by the Wisconsin ERC (Kokjohn et al., 2011, 2012; Splitter et al., 2010, 2012). Essentially, using two fuels with different reactivities qualifies as RCCI, but this specific strategy involves dividing the diesel fuel into two injections to maximize the stratification of reactivity. This approach has significantly improved thermal efficiency compared to the conventional diesel-pilot dual-fuel combustion and offers advantages in reducing both smoke and  $\text{NO}_x$  emissions.

According to the research by Kokjohn et al., they have achieved a gross indicated thermal efficiency (GIE) of over 50% in large compression ignition engines through gasoline and diesel RCCI combustion (Kokjohn et al., 2011). They have also expanded the maximum load, based on the highest rate of pressure rise in the combustion chamber, up to a maximum gross indicated mean effective pressure (gIMEP) of 1.6 MPa. On the other hand, according to the research by Benajes et al., they have mapped the combustion based on homogeneous charge by optimizing the degree of reactivity stratification in the combustion chamber through diesel injection timing, reaching gIMEP values exceeding 2.0 MPa under high-load operating conditions (Benajes et al., 2017). However, both studies were conducted using conventional gasoline and diesel fuels and not alternative fuels.

In this regard, several previous studies, including the Wisconsin ERC group, have utilized natural gas as a low-reactivity fuel. Nieman et al. explored the possibility of RCCI combustion up to gIMEP of 1.9 MPa through interpretation and some experimental research (Nieman et al., 2012). Other previous studies mainly focused on load expansion through extending the knocking limit of dual-fuel combustion or reducing smoke emissions (Wang et al., 2016; Wei & Geng, 2016; Zhang et al., 2017). In the case of liquid alternative fuels, ethanol was used as a low-reactivity fuel, and research primarily focused on improving low-load RCCI combustion, unlike the previous natural gas-diesel RCCI combustion. Ethanol, with lower calorific value compared to gasoline or natural gas, was mainly studied under low-load conditions, and results were derived based on the fuel substitution ratio.

Particularly, Pedrozo et al. expanded the range up to gIMEP of 0.3 MPa in ethanol–diesel RCCI combustion, achieving a GIE level of around 36–41% using internal exhaust gas recirculation (EGR) (Pedrozo et al., 2016). Meanwhile, Lee et al. confirmed an approximate 42% GIE level between gIMEP level of 0.2–0.8 MPa under ethanol–diesel direct injection RCCI combustion conditions, also discussing the size of smoke emissions (Lee et al., 2018).

However, there is a lack of previous studies that comparatively analyze the combustion characteristics of low-reactivity fuels under both low-load and mid-load conditions. Particularly, experimental results evaluating the effect of carbon dioxide reduction through low-carbon fuels in the era of carbon neutrality are needed. Therefore, in this study, experimental investigations were conducted on combustion, thermal efficiency, and exhaust characteristics by varying low-reactivity fuels such as gasoline, ethanol, and propane in the same compression ignition engine, optimizing each operating condition under four different load conditions.

## Experimental Setup and Condition

### Experimental Setup

In these experiments, a single-cylinder diesel engine was used. This engine had a displacement of 0.4 L and featured a compression ratio of 14, specifically configured to reduce  $\text{NO}_x$  emissions. To inject fuel, a solenoid diesel injector capable of spraying at pressures up to 180 MPa was employed alongside a common rail system. Additionally, two solenoid gasoline port fuel injectors (PFIs) were installed on the intake port, operating at a fuel pressure of 0.5 MPa. Gasoline and ethanol were delivered through these PFIs, while propane was introduced into the intake port as a gaseous substance at a pressure of 0.3 MPa. The propane flow rate was controlled using sonic orifices via choke flow. The ratio of diesel to low-reactivity fuels (LRFs) was determined based on mass measurements. You can find detailed specifications of the engine in Table 1. The engine's operation was regulated by a 37 kW DC dynamometer. Flow rates of diesel, gasoline, and ethanol were measured using a

**Table 1** Engine specifications

Engine type	Single cylinder (four-stroke) compression ignition
Displacement (L)	0.4
Bore × stroke (mm)	77.2 × 84.5
Connecting rod (mm)	140
Compression ratio (-)	14

mass burette-type flowmeter (ONO SOKKI, FX-203P) and a mass flow meter (AVL, 7030 flow meter), respectively. Meanwhile, a gas flow meter (MK Precision Co., MFM (TSM-230)) was used to measure propane. The air-to-fuel ratio (AFR) was continuously monitored by an oxygen sensor (Horiba, MEXA 110Lambda) located on the exhaust manifold. Airflow rates were calculated considering the fuel ratio between each LRF and diesel, taking into account the measured AFR.

To assess the exhaust gas composition, an exhaust gas analyzer (Horiba, MEXA 7100DEGR) was employed to measure the concentrations of  $\text{NO}_x$ , total hydrocarbons (THC), CO,  $\text{CO}_2$ , and  $\text{O}_2$ . Smoke emissions were evaluated using a smoke meter (AVL, 415S). Both Exhaust Gas Recirculation (EGR) and air were pressurized simultaneously using an independent supercharger, effectively simulating a low-pressure (LP) EGR system. Subsequently, the EGR and air mixture was cooled through an intercooler system, and EGR rates were adjusted using an EGR valve. EGR

rates were computed based on volumetric values derived from the  $\text{CO}_2$  fractions in the exhaust and intake gases. Pressure measurements were conducted using an absolute pressure transducer (Kistler, 4045A5), while a relative pressure transducer (Kistler, 6055Bsp) was employed to determine in-cylinder pressure. Data from these pressure transducers were recorded at intervals of one crank angle per 200 cycles for each test scenario using a data acquisition system (Kistler, KiBox To Go 2893). The experimental setup is visually depicted in Fig. 1, and you can find fundamental characteristics of each fuel in Table 2. The Gross Indicated Efficiency (GIE) and combustion loss were computed using Eqs. 1–4 (Kokjohn et al., 2012).

$$\text{GIE} = \frac{W_{\text{gross}}}{m_{\text{gasoline}} \times Q_{\text{LHV of gasoline}} + m_{\text{diesel}} \times Q_{\text{LHV of diesel}}}, \quad (1)$$

$$\text{Combustion loss} = \frac{m_{\text{THC of each cycle}} \times Q_{\text{LHV avg of fuel}} + m_{\text{CO of each cycle}} \times Q_{\text{LHV of CO}}}{m_{\text{low reactivity fuel}} \times Q_{\text{LHV of low reactivity fuel}} + m_{\text{diesel}} \times Q_{\text{LHV of diesel}}}, \quad (2)$$

$$\text{Heat transfer loss} = \frac{(m_{\text{LRF}} \times Q_{\text{LHV of LRF}} + m_{\text{diesel}} \times Q_{\text{LHV of diesel}}) \times (1 - \text{combustion loss}) - \text{Cumulative HR}}{m_{\text{LRF}} \times Q_{\text{LHV of LRF}} + m_{\text{diesel}} \times Q_{\text{LHV of diesel}}}, \quad (3)$$

$$\text{Exhaust loss} = 1 - (\text{GIE}) - (\text{combustion loss}) - (\text{heat transfer loss}). \quad (4)$$

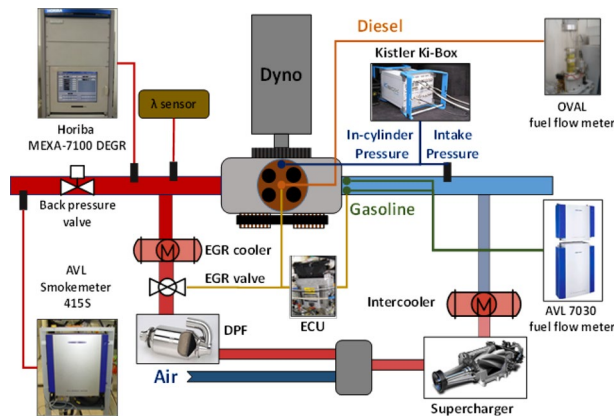


Fig. 1 Schematic diagram of experimental setup

## Experimental Conditions

Four representative operating conditions as various engine speeds and gIMEP conditions were selected for this research. There were four constraints about gross indicated specific  $\text{NO}_x$  ( $\text{gISNO}_x$ ) below 0.15 g/kWh, smoke emission below 15 mg/kWh, the maximum in-cylinder pressure rise rate ( $\text{PRR}_{\text{max}}$ ) below 1 MPa/deg and CoV of gIMEP lower than 3%.

Table 2 Properties of diesel, gasoline, ethanol and propane

Properties	Diesel	Gasoline	Ethanol	Propane
Chemical formula	$\text{C}_x\text{H}_{2.0x}$	$\text{C}_x\text{H}_{2.0x}$	$\text{CH}_3\text{CH}_2\text{OH}$	$\text{C}_3\text{H}_8$
Density ( $\text{g}/\text{cm}^3$ )	0.831 (liquid)	0.724 (liquid)	0.789 (liquid)	$1.808 \times 10^{-3}$ (gas)
Low heating value (MJ/kg)	44.0	42.8	26.8	46.4
Cetane/octane number	54 (CN)	91 (RON)	113 (RON)	112 (RON)
Auto-ignition temp. (K)	483	520–553	638	723
Stoichiometric ratio (wt%)	14.6	14.5	9.0	15.5
Adiabatic temperature@ stoichiometric condition (K)	~2270	2411	2355	2523
The maximum laminar flame speed (cm/s)	None	42	48	45

The four experimental conditions were determined in consultation with the engine manufacturer as representative operating conditions for low-to-medium loads. In addition, the exhaust emission constraint and combustion stability criteria were also modified to fit the single-cylinder engine experiments, taking into account the engine manufacturer’s guidelines and EURO-VI emission regulations. These constraints were satisfied by controlling the fuel ratios between each LRF and diesel, diesel start of injection (SOI), EGR rate. For all the test, single diesel injection was applied, and its injection pressure was fixed as 45 MPa. Detailed experimental conditions are introduced in Table 3.

## Results and Discussion

### Combustion Analysis

Figure 2 illustrates the energy supply reference ratio (a) and EGR rate (b) of low-reactivity fuel across four distinct operational scenarios, all aligned with the requirements for minimizing NO<sub>x</sub> and smoke while regulating combustion. To curtail NO<sub>x</sub> emissions, it becomes imperative to either prolong the ignition delay phase to extend the premixing interval or diminish the oxygen concentration in the intake air (Heywood, 1988). As detailed in Table 2, for propane,

**Table 3** Experimental conditions

Common variables				
Parameter	Specification			
Case number	1	2	3	4
Engine speed (rpm)	1500	1750	2000	2000
gIMEP (MPa)	0.52	0.74	0.95	1.15
Overall equivalence ratio $\Phi$ (-)	0.62	0.74	0.91	0.88
Intake air temperature (K)	298			
Coolant and oil temperature (K)	358			
Diesel injection pressure (MPa)	45			
Varied as low reactivity fuels				
Low reactivity fuel injection pressure (MPa)	Gasoline/ethanol 0.5 Propane 0.3			
Low reactivity fuel port SOI (°BTDC)	Gasoline/ethanol 60 Propane: fumigation			
Diesel DI SOI (°BTDC)	30			
EGR rate (%)	Varied according to operating conditions (from 37 to 50)			
Constraints				
gISNO <sub>x</sub> (g/kWh)	0.15			
gISSmoke (mg/kWh)	15			
PRRmax (MPa/deg)	1			
CoV of gIMEP (%)	3			

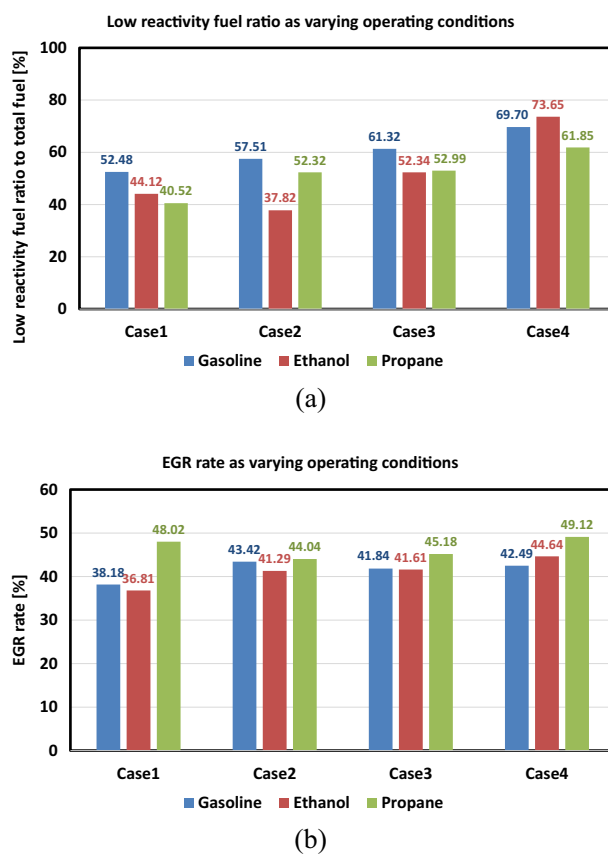


**Fig. 2** Low reactivity fuel ratios to total fuel based on LHV (a) and EGR rate (b) as varying LRFs under four different cases

possessing a relatively elevated adiabatic flame temperature, a heightened EGR rate was employed to curtail oxygen concentration, thereby enhancing ignition stability when employing a higher proportion of diesel in comparison to gasoline (Lee et al., 2017, 2019). Augmenting the EGR rate effectively curbs NO<sub>x</sub> emissions, albeit potentially fostering increased smoke when the diesel fraction is substantial. Yet, due to propane’s gaseous nature, there exists leeway for smoke emissions, thereby enabling EGR optimization.

Conversely, in the case of ethanol, as indicated in Table 2, its Research Octane Number (RON) akin to propane inherently permits a protracted ignition delay phase. Moreover, ethanol inherently contains oxygen within its composition, translating to less encumbrance in terms of smoke emissions. Thus, as demonstrated in Fig. 2a, during ethanol/diesel RCCI combustion (E/D), analogous to propane, a lower diesel fraction was adopted, negating the necessity for an exceedingly high EGR rate employed in propane for NO<sub>x</sub> reduction. Lastly, for gasoline/diesel RCCI combustion (G/D), in the pursuit of concurrent NO<sub>x</sub> and smoke reduction, the gasoline fraction was heightened to reach 52.48%.

As depicted in Fig. 3a, during low-load conditions (case 1), the combustion characteristics of G/D facilitated

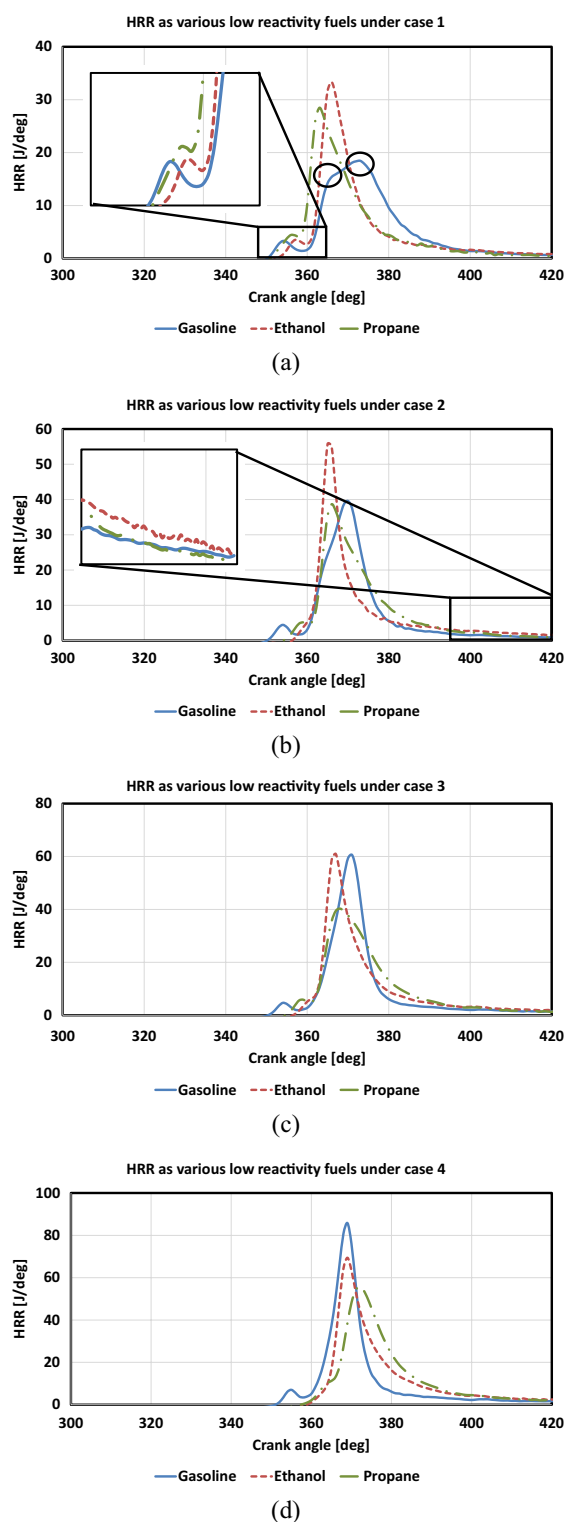


**Fig. 3** HRR as various LRFs under case 1 (a), case 2 (b), case 3 (c) and case 4

a reduction in combustion chamber temperature due to the retardation of combustion phase. This yielded a heightened peak heat release rate (HRR) and a more compact premixed combustion phase for ethanol and propane

compared to gasoline, which manifested relatively lower peak HRR and exhibited twin peaks in HRR. In case 1, the low-temperature heat release (LTHR) region, emblematic of premixed combustion, was distinctly observable. Yet, with escalating load, the LTHR region was only conspicuous in  $G/D$  (Waqas et al., 2019).

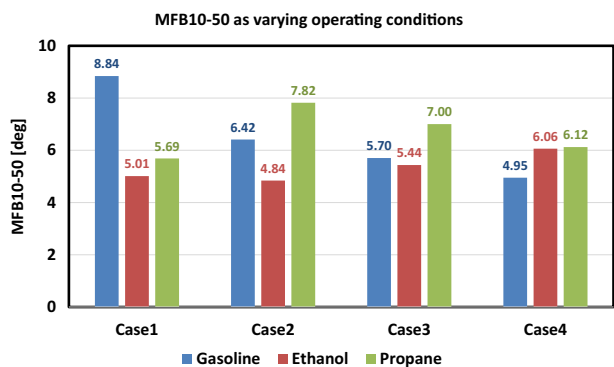
With heightened load, the twin peaks in HRR coalesced into the prototypical shape of RCCI combustion HRR, evident in Fig. 3d for case 4 (Lee et al., 2019). This canonical RCCI combustion HRR pattern features a well-defined LTHR segment followed by a gradual initial HRR rise, succeeded by a rapid ascent after the peaks (Reitz & Duraisamy, 2015). Amplifying the load simultaneously augmented the supply proportion of low-reactivity fuel, consequently expediting the start of combustion (SOC) for  $G/D$  due to its comparably low RON and auto-ignition temperature.

A more exhaustive analysis of combustion metrics is presented in Fig. 4. The primary combustion interval is presented in Fig. 4. The primary combustion interval was defined as the mass fraction burned from 10 to 90% (MFB10-90), further partitioned into early combustion (MFB10-50) and late combustion (MFB50-90) phases (Fig. 4a, b, respectively). Generally, MFB10-50 remained consistent around  $5^{\circ}$ – $7^{\circ}$  for most instances, barring case 1 with a relatively modest diesel fraction where it slightly extended. Figure 4b indicates that the late combustion (MFB50-90) for gasoline and propane was akin, while ethanol displayed a lengthier duration. Despite similar laminar flame speed among fuels (as shown in Table 2), differences in localized premixing within the combustion chamber, stemming from propane's gaseous supply versus ethanol's liquid delivery through PFI, conceivably influenced the late combustion phase.

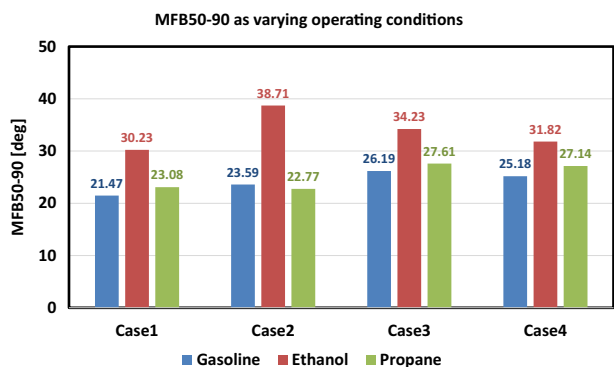
Figure 4c employs the MFB50 point as a reference, unveiling that the engine employed in the study exhibited optimal thermal efficiency around  $7$ – $10^{\circ}$  ATDC for MFB50. Nevertheless, certain circumstances necessitated retarding the MFB50 point to align with  $\text{NO}_x$  limitation constraints. Figure 5 delineates the ignition delay period for distinct fuels, commencing from the diesel fuel's start of injection (SOI) to MFB10.  $G/D$  generally upheld an ignition delay of approximately  $33^{\circ}$  regardless of load conditions. Conversely, for ethanol and propane, the ignition delay phase elongated with escalating load and output.

Figure 5 delineates the ignition delay period for distinct fuels, commencing from the diesel fuel's start of injection (SOI) to MFB10.  $G/D$  generally upheld an ignition delay of approximately  $33^{\circ}$  regardless of load conditions. Conversely, for ethanol and propane, the ignition delay phase elongated with escalating load and output.

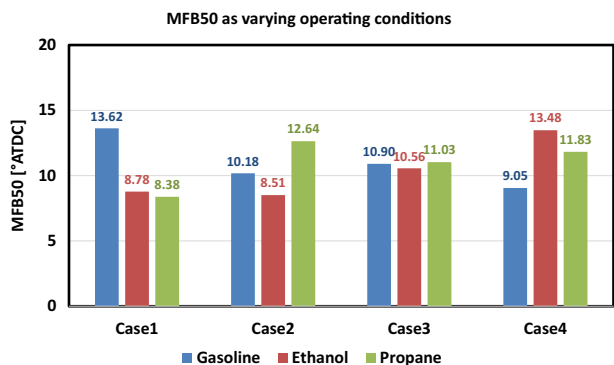
In contrast, Fig. 6 charts the maximum in-cylinder pressure rise rate ( $\text{PRR}_{\text{max}}$ ), which adheres to the stipulated  $1 \text{ MPa}/^{\circ}$  limitation for all fuels. The  $\text{PRR}_{\text{max}}$  expanded with



(a)



(b)



(c)

Fig. 4 MFB10-50 (a), MFB50-90 (b) durations and MRB 50 (c) as varying LRFs under four different cases

increased load across all scenarios. Ethanol registered a higher  $PRR_{max}$ , while propane maintained a relatively subdued  $PRR_{max}$ , not exceeding  $0.65 \text{ MPa}/^\circ$ .

**Emissions and Efficiency Analysis**

Across all scenarios,  $NO_x$  and smoke emissions were already at levels within  $0.15 \text{ g/kWh}$  and  $15 \text{ mg/kWh}$ , respectively. Hence, our primary focus will be on  $CO_2$ ,  $CO$ , and  $THC$  emissions.

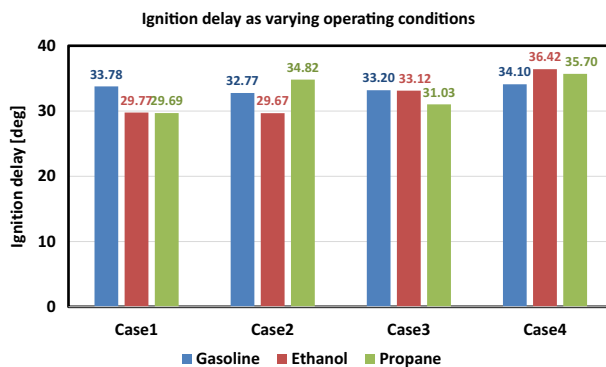


Fig. 5 Ignition delay (from diesel SOI to MFB10) as varying LRFs under four different cases

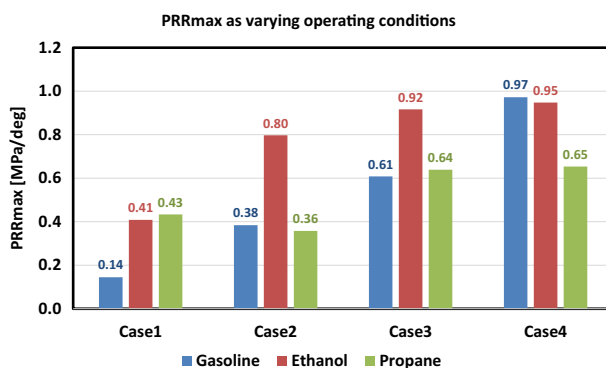


Fig. 6 PRRmax as varying LRFs under four different cases

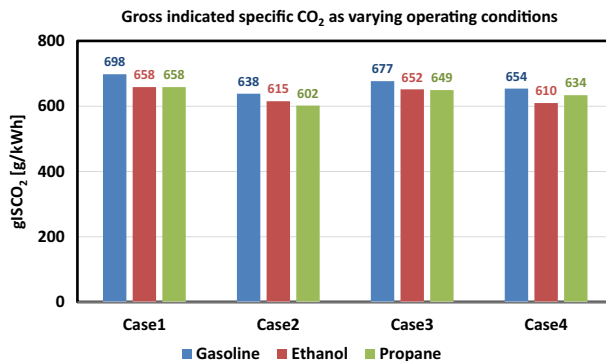
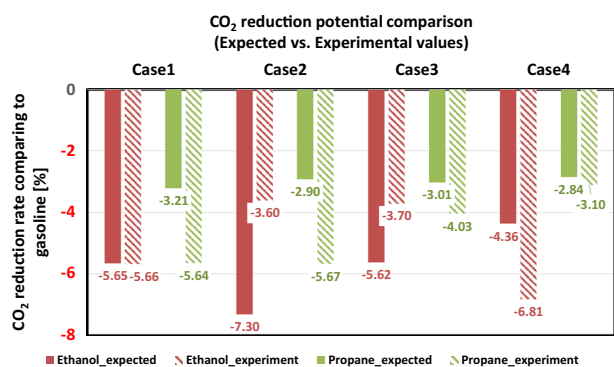


Fig. 7  $gISCO_2$  as varying LRFs under four different cases

Figure 7 displays the gross indicated specific  $CO_2$  ( $gISCO_2$ ) based on diverse fuels and driving conditions. Upon replacing gasoline with low-carbon options like ethanol and propane as low-reactivity fuels, a noteworthy reduction in  $CO_2$  emissions becomes evident regardless of driving conditions. Nevertheless, the magnitude of this reduction varies depending on factors such as the



**Fig. 8** CO<sub>2</sub> reduction potential comparison between expected and experimental values

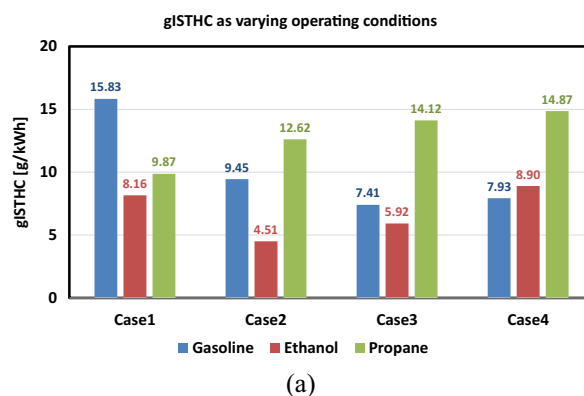
substitution rate of low-reactivity fuels, GIE, and EGR rate. Notably, during Case 2 conditions, propane/diesel RCCI combustion (*P/D*) demonstrated the lowest CO<sub>2</sub> emissions at 601 g/kWh, while under maximum power conditions (Case 4), *E/D* achieved a CO<sub>2</sub> emission reduction of up to 609 g/kWh.

To validate this reduction, Fig. 8 compares projected values with actual experimental data to assess the reduction rate. Projected values are computed based on chemical reaction equations for gasoline and diesel, assuming iso-octane (C<sub>8</sub>H<sub>18</sub>) as the component with the smallest carbon number. Assuming complete combustion of 1 mol of each low-reactivity fuel, gasoline (assumed as iso-octane) yields 8 mol of CO<sub>2</sub>, ethanol yields 2 mol, and propane yields 3 mol. Considering these results in terms of volume, the CO<sub>2</sub> emission ratio from complete combustion of 1 kg of fuel is approximately 3.08:1.76:3.00 for gasoline, ethanol, and propane, respectively. Consequently, the CO<sub>2</sub> reduction potential is formulated and calculated relative to *G/D* as follows:

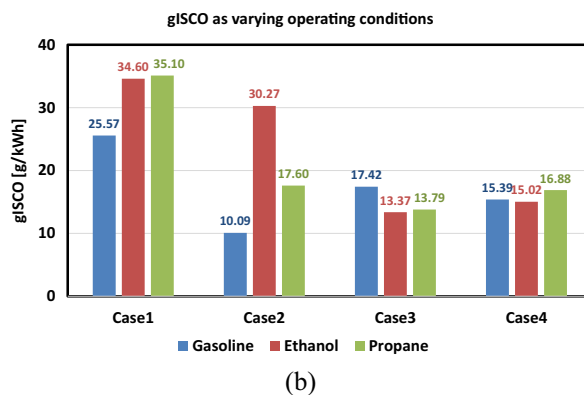
$$\text{CO}_2 \text{ reduction potential} = \frac{\text{CO}_2 \text{ mass from C}_8\text{H}_{18} - \text{CO}_2 \text{ mass from E or P}}{\text{CO}_2 \text{ mass from C}_8\text{H}_{18}} \times \text{LRF substitution ratio} \times \frac{\text{GIE of E/D or P/D}}{\text{GIE of G/D}}. \quad (5)$$

The findings reveal that expected values aligned closely with experimental data for Case 1 conditions, and marginal discrepancies were noted for other driving conditions. Particularly, under Case 2, 3, and 4 conditions, both *P/D* and *E/D* exhibited even more pronounced CO<sub>2</sub> reduction effects than anticipated values. However, this is likely attributed to the increase in non-methane hydrocarbons emitted, which were not emitted as CO<sub>2</sub>, as elaborated later.

Figure 9 illustrates THC and CO emissions. In Fig. 9a, barring case 1 with combustion phasing issues in *G/D*, *P/D* exhibited elevated THC emissions. This can be attributed



(a)



(b)

**Fig. 9** gISTHC (a) and gISCO (b) results as varying LRFs under four different cases

to propane's gaseous supply, which reduces combustion efficiency due to the crevice effect compared to the two liquid fuels. Conversely, in the case of *E/D*, the inherent oxygen content within ethanol fuel translated to lower THC emissions.

Regarding CO emissions in Fig. 9b, comparatively high emissions were observed for *E/D* under low-load conditions (case 1 and case 2). Specifically, under case 1 (low-load condition), both ethanol and propane exhibited higher CO emissions than gasoline. In case 2, ethanol displayed notably higher CO emissions. As deduced from Fig. 4b, where the MFB50-90 period appeared elongated for *E/D*, it is hypothesized that inadequate air and premixing within the combustion chamber led to localized rich regions, impeding smooth combustion and resulting in CO emissions. CO is contingent upon local equivalence ratios, suggesting that mixture preparation is at the core of this issue.

Lastly, Fig. 10 presents the energy distribution for distinct fuels across the four operating conditions. Although variations in GIE between fuels are not drastic, ethanol and propane applications demonstrate clearer GIE enhancements in case 1 and case 4. In case 1, combustion losses of 13.54% were encountered in *G/D* due to



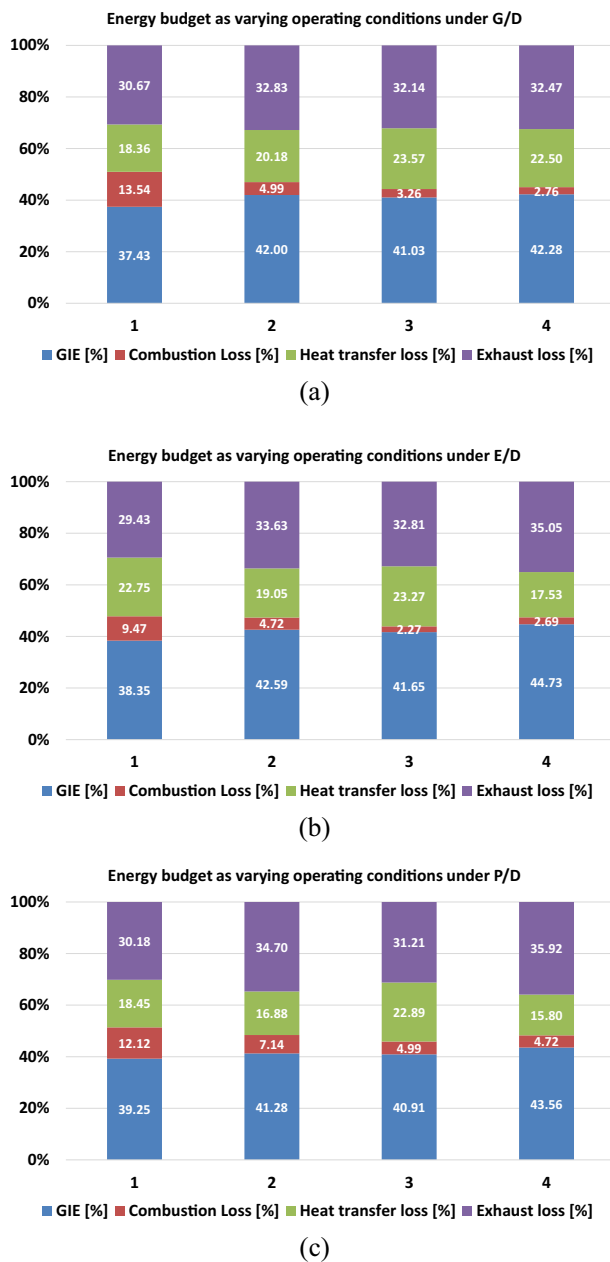


**Fig. 10** Energy budget as varying operating conditions under using gasoline (a), ethanol (b) and propane (c)

combustion phasing challenges and heightened exhaust enthalpy losses, leading to diminished GIE. Conversely, *P/D* incurred combustion losses of 12.21%, yet maintained a margin for heat transfer losses within the combustion chamber due to elevated EGR rates, bolstering thermal efficiency. *E/D* showcased the lowest combustion losses in all operating conditions, showcasing the advantages of its combustion efficiency, buoyed by a lower EGR rate, higher diesel fraction, and oxygen content in ethanol fuel, contributing to overall GIE enhancement. Across all operating

conditions, *P/D* exhibited exacerbated combustion losses due to factors such as the crevice effect.

### Conclusions

In this investigation, the feasibility of using gasoline, ethanol, and propane as low-reactivity fuels in RCCI combustion to mitigate CO<sub>2</sub> emissions was explored across four distinct driving conditions. Each condition adhered to four specific constraints: nitrogen oxides, smoke, PRR<sub>max</sub>, and CoV of gIMEP. The summarized research findings are outlined as follows:

1. In the case of *P/D*, the relative diesel fraction was heightened, and the EGR rate was increased to extend the premixing phase, leading to decreased NO<sub>x</sub> and smoke emissions. In contrast, *G/D*, where liquid fuel injection was employed, exhibited improved premixed combustion with a greater proportion of low-reactivity gasoline. Ethanol, due to its inherent oxygen content, operated comfortably at relatively low EGR rates and ethanol fractions, especially during low-load conditions, without smoke emission concerns. Moreover, while there were minimal differences in the MFB10-50 period among fuels, *E/D* displayed a slightly accelerated trend. Conversely, *E/D* exhibited the slowest MFB50-90 period, and the rate of combustion pressure rise was most pronounced in *E/D*.
2. Ethanol and propane, as low-reactivity fuels, showcased the ability to reduce CO<sub>2</sub> emissions compared to *G/D*, across varied load conditions. In both *E/D* and *P/D* setups, the reduction hovered around 5.64% during low-load conditions and reached up to about 6.81% in *E/D* under high-load conditions compared to *G/D*. The rate of CO<sub>2</sub> emission reduction via low-reactivity fuel substitution in RCCI combustion closely aligned between projected and actual data. Different driving conditions yielded comparable GIE regardless of the low-reactivity fuel employed. However, *E/D* demonstrated a slight advantage in terms of combustion losses. Particularly at 1500 rpm/gIMEP 0.52 MPa conditions, where the need to meet nitrogen oxides limits caused delayed combustion in *G/D*, resulting in heightened combustion losses.
3. Contrary to expectations, the reduction in CO<sub>2</sub> emissions was less significant than anticipated. Given the dual-fuel nature of this combustion method alongside diesel, achieving higher substitution rates of low-reactivity fuel requires raising the compression ratio. However, this elevation might inadvertently lead to increased NO<sub>x</sub> emissions, underscoring the importance of judiciously leveraging EGR and managing the air–fuel ratio. While

the low-carbon fuel combustion method indeed holds potential for effective CO<sub>2</sub> reduction, comprehensive research into their utilization in compression-ignition engines should factor in these considerations to optimize engine thermal efficiency.

**Acknowledgements** This research was supported by the Hyundai Motor Company and Seoul National University Institute of Advanced Machines and Design (SNU IAMD). In addition, this study was also supported by the National Research Foundation of South Korea (NRF) (no. 2021R1G1A1004451/Investigation into the hydrogen fueled lean SPCCI combustion engine by developing operating strategy and hardware) and the Ministry of Trade, Industry and Energy of South Korea (MOTIE) (no. 20018473/Development of Direct Injection Hydrogen Engine Source Technology based on Carbon-Free Hydrogen Fuel) in the aspect of conceptualization, data analysis and draft.

**Funding** Open Access funding enabled and organized by Seoul National University.

**Data availability** The datasets used and/or analysed during the current study available from the corresponding author on reasonable request.

**Open Access** This article is licensed under a Creative Commons Attribution 4.0 International License, which permits use, sharing, adaptation, distribution and reproduction in any medium or format, as long as you give appropriate credit to the original author(s) and the source, provide a link to the Creative Commons licence, and indicate if changes were made. The images or other third party material in this article are included in the article's Creative Commons licence, unless indicated otherwise in a credit line to the material. If material is not included in the article's Creative Commons licence and your intended use is not permitted by statutory regulation or exceeds the permitted use, you will need to obtain permission directly from the copyright holder. To view a copy of this licence, visit <http://creativecommons.org/licenses/by/4.0/>.

## References

- Ayman, E., Shixing, W., Thibault, G., & William, R. (2022). Review on the recent advances on ammonia combustion from the fundamentals to the applications. *Fuel Communications*, 10, 100053.
- Benajes, J., Garcia, A., Monsalve-Serrano, J., & Boronat, V. (2017). Achieving clean and efficient engine operation up to full load by combining optimized RCCI and dual-fuel diesel-gasoline combustion strategies. *Energy Conversion and Management*, 136, 142–151.
- Felayati, F., Semin, C. B., Bakar, R., & Birouk, M. (2021). Performance and emissions of natural gas/diesel dual-fuel engine at low load conditions: Effect of natural gas split injection strategy. *Fuel*, 300, 121012.
- Heywood, J. (1988). *Internal combustion engine fundamentals*. McGraw-Hill.
- Karim, G. (1980). A review of combustion processes in the dual fuel engine—The gas diesel engine. *Progress in Energy and Combustion Science*, 6(3), 277–285.
- Karim, G. (2015). *Dual-fuel diesel engines*. CRC Press.
- Lee, J., Chu, S., Cha, J., Choi, H., & Min, K. (2015). Effect of the diesel injection strategy on the combustion and emissions of propane/diesel dual fuel premixed charge compression ignition engines. *Energy*, 93, 1041–1052.
- Lee, J., Chu, S., Kang, J., Min, K., Jung, H., Kim, H., & Chi, Y. (2017). Operating strategy for gasoline/diesel dual-fuel premixed compression ignition in a light-duty diesel engine. *International Journal of Automotive Technology*, 18(6), 943–950.
- Lee, J., Chu, S., Kang, J., Min, K., Jung, H., Kim, H., & Chi, Y. (2019). The classification of gasoline/diesel dual-fuel combustion based on the heat release rate shapes and its application in a light-duty single-cylinder engine. *International Journal of Engine Research*, 20(1), 69–79.
- Lee, J., & Lee, B. (2022). Survey on research and development of E-fuel. *Journal of the Korean Society Combustion*, 27(1), 37–57.
- Lee, J., Lee, S., & Lee, S. (2018). Experimental investigation on the performance and emissions characteristics of ethanol/diesel dual-fuel combustion. *Fuel*, 220, 72–79.
- Pedrozo, V., May, I., Lanzanova, T., & Zhao, H. (2016). Potential of internal EGR and throttled operation for low load extension of ethanol–diesel dual-fuel reactivity controlled compression ignition combustion on a heavy-duty engine. *Fuel*, 179, 391–405.
- Reitz, R., & Duraisamy, G. (2015). Review of high efficiency and clean reactivity controlled compression ignition (RCCI) combustion in internal combustion engines. *Progress in Energy and Combustion Science*, 46, 12–71.
- Wang, Z., Zhao, Z., Wang, D., Tan, M., Han, Y., Liu, Z., & Dou, H. (2016). Impact of pilot diesel ignition mode on combustion and emissions characteristics of a diesel/natural gas dual fuel heavy-duty engine. *Fuel*, 167, 248–256.
- Waqas, M., Hoth, A., Kolodziej, C., Rockstroh, T., Gonzalez, J., & Johansson, B. (2019). Detection of low temperature heat release (LTHR) in the standard Cooperative Fuel Research (CFR) engine in both SI and HCCI combustion modes. *Fuel*, 256, 115745.
- Wei, L., & Geng, P. (2016). A review on natural gas/diesel dual fuel combustion, emissions and performance. *Fuel Processing Technology*, 142, 264–278.
- Zhang, C., Zhou, A., Shen, Y., Li, Y., & Shi, Q. (2017). Effects of combustion duration characteristic on the brake thermal efficiency and NO<sub>x</sub> emission of a turbocharged diesel engine fueled with diesel-LNG dual-fuel. *Applied Thermal Engineering*, 127, 312–318.
- Climate Watch, the World Resources Institute. (2020). Our world in data.
- Inagaki, K., Fuyuto, T., Nishikawa, K., Nakakita, K., & Sakata I. (2006). Dual-fuel PCI combustion controlled by in-cylinder stratification of ignitability. *SAE Technical Paper 2006-01-0028*.
- IPCC special report. (2018). Global warming of 1.5 °C. <https://www.ipcc.ch/sr15>
- Kokjohn, S., Hanson, R., Splitter, D., Kaddatz, J., & Reitz, R. (2011). Fuel reactivity controlled compression ignition (RCCI) combustion in light- and heavy-duty engines. *SAE Technical Paper 2011-01-0357*
- Kokjohn, S., Reitz, R., Splitter, D., & Musculus, M. (2012). Investigation of fuel reactivity stratification for controlling PCI heat-release rates using high-speed chemiluminescence imaging and fuel tracer fluorescence. *SAE Technical Paper 2012-01-0375*.
- Nieman, D., Dempsey, A., & Reitz, R. (2012). Heavy-duty RCCI operation using natural gas and diesel. *SAE Technical Paper 2012-01-0379*.
- Splitter, D., Reitz, R., & Hanson, R. (2010). High efficiency, low emissions RCCI combustion by use of a fuel additive. *SAE Technical Paper 2010-01-2167*.
- Splitter, D., Wissink, M., Kokjohn, S., & Reitz, R. (2012). Effect of compression ratio and piston geometry on RCCI load limits and efficiency. *SAE Technical Paper 2012-01-0383*.

**Publisher's Note** Springer Nature remains neutral with regard to jurisdictional claims in published maps and institutional affiliations.